# The Determination of Sky View-Factors in Urban Environments Using Video Imagery

D. G. STEYN AND J. E. HAY

*Department of Geography, University of British Columbia, Vancouver, B.C. Canada V6T 1W5*

IAN D. WATSON AND GLENN T. JOHNSON

*Macquarie University, North Ryde 2113 NSW, Australia*

13 January 1986 and 23 June 1986

ABSTRACT

A technique is described whereby sky view-factors may be determined using a video camera equipped with a fish-eye lens. The video image is digitized and then analyzed to distinguish between "sky" and "non-sky" pixels. View-factors are calculated for each pixel and then summed for all "sky" pixels to yield a composite sky view-factor for the image. The technique is illustrated by applying it in three urban locations, all of which are characterized by high building densities (and hence complex skylines). The three images processed have sky view-factors in the range 0.15 to 0.46 (as independently determined). It is shown that the present technique produces values in close agreement with these and appears quite robust when compared with calculations based on the work of Johnson and Watson.

## 1. Introduction

Estimation of radiant heat exchange in complex environments, such as "urban canopies," where the distribution of longwave or diffuse radiation is clearly anisotropic, has led to an interest in view-factors, whereby the proportion of radiation received by a surface from surrounding, uniquely radiating surfaces may be determined. Thus, it is possible to estimate the proportion of longwave radiation received at the floor of an urban canyon from surrounding walls and sky by calculating sky and wall view-factors for an element at the canyon floor (Oke, 1981; Johnson and Watson, 1984).

View-factors may be calculated for individual walls in urban canyons using the analytical results of Johnson and Watson (1984), Steyn and Lyons (1985), and Johnson and Watson (1985a), but it is more convenient to use photographic techniques when the radiating surfaces are numerous. One such approach has been to use a fish-eye lens to produce an equiangular hemispheric projection of the radiating environment. Anderson (1964) applied the technique in forest canopies by overlaying the circular fish-eye lens image with a polar grid, where each grid cell represented 0.1% of the total illuminance from an overcast sky. A sky view-factor may be determined for a horizontal element by summing all the clear-sky grid cells in the photograph and dividing by the total number of grid cells in the circular image. An alternative approach was proposed by Steyn (1980) for use in urban environments. Steyn divided the circular fish-eye lens image into 40 annuli and calculated the view-factor for the azimuthal angular extent of each annulus. This required redrawing the image boundaries in a stepwise manner to coincide with the appropriate annuli. Johnson and Watson (1984) took a similar approach to Steyn's but showed that it was possible to determine wall view-factors by specifying the polar coordinates of each wall-end in the photograph. These data may be acquired quickly by placing the photograph on a digitizing tablet and locating the wall-ends of each building in the image.

Each of the above approaches requires a degree of manual intervention which may prove prohibitive if view-factors are required for many locations in complex skylines. In this respect, we propose a technique whereby sky and wall view-factors may be obtained in a more automated fashion from video images. The method requires that an image produced by a video camera equipped with a fish-eye lens be digitized by a frame-store device into an array of pixels, each with an ascribed brightness level. The view-factor of each pixel is calculated and then summed for all pixels within a range of brightness levels corresponding to an identifiable surface in the radiating environment.

## 2. View-factors of pixels

It is first necessary to determine the view-factor of each pixel in the circular image produced by the fish-eye lens. For a horizontal planar element at the center of the image, the view-factor of an area, P′, on the surface of a hemisphere of radius $r_0$ centered on the image may be defined in terms of its equiangular projection, P, on the circular image as

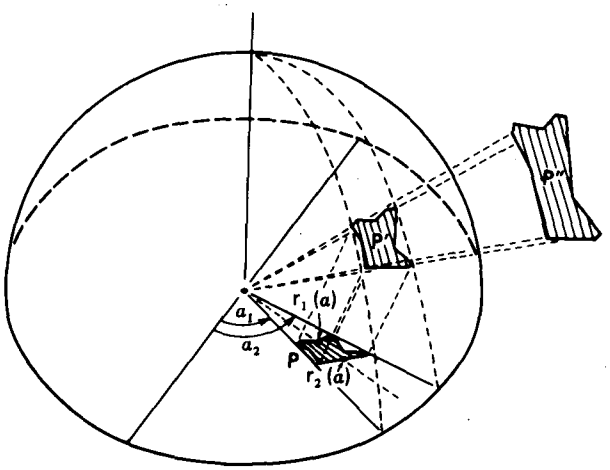


FIG. 1. Schematic projection of an area P″, through a hemisphere (via P′) to the image (P) on the image plane.

$$\psi_P = \frac{1}{2r_0}\int_P \sin\frac{\pi r}{2r_0}\cos\frac{\pi r}{2r_0}\,dr d\alpha \tag{1}$$

where $r_0$ is the radius of the image and $r$ and $\alpha$ are polar coordinates defining points in P (Fig. 1). Equation (1) may be simplified to

$$\psi_P = \frac{1}{4r_0}\int_P \sin\frac{\pi r}{r_0}\,dr d\alpha \tag{2}$$

$$= \frac{1}{4r_0}\int_{\alpha_1}^{\alpha_2}\int_{r_1(\alpha)}^{r_2(\alpha)} \sin\frac{\pi r}{r_0}\,dr d\alpha \tag{3}$$

$$= \frac{1}{4\pi}\int_{\alpha_1}^{\alpha_2}\left[\cos\frac{\pi}{r_0}r_1(\alpha) - \cos\frac{\pi}{r_0}r_2(\alpha)\right]d\alpha \tag{4}$$

$$= \psi(\alpha_1, \alpha_2, r_1(\alpha), r_2(\alpha)). \tag{5}$$

Equation 4 may be evaluated numerically once the limits $\alpha_1$, $\alpha_2$ and functions $r_1(\alpha)$, $r_2(\alpha)$ are specified. In the present application, the area P is given by individual pixels that usually have a rectangular geometry because of the aspect (height:width) ratio of the video image. In this case the integration is performed over azimuth angles and radii that define the edges of the rectangle.

However, the integration is not as straightforward as Fig. 2 illustrates for just one possible position of a pixel with respect to the center of the image. For ease of computation, Eq. 4 may be evaluated separately for three segments of the pixel shown in Fig. 2 such that

$$\psi_P = \psi_\alpha(\alpha_1, \alpha_2, c/\sin\alpha, b/\cos\alpha) + \psi_\beta(\beta_1, \beta_2, c/\sin\beta, d/\sin\beta) + \psi_\gamma(\gamma_1, \gamma_2, a/\cos\gamma, d/\sin\gamma). \tag{6}$$

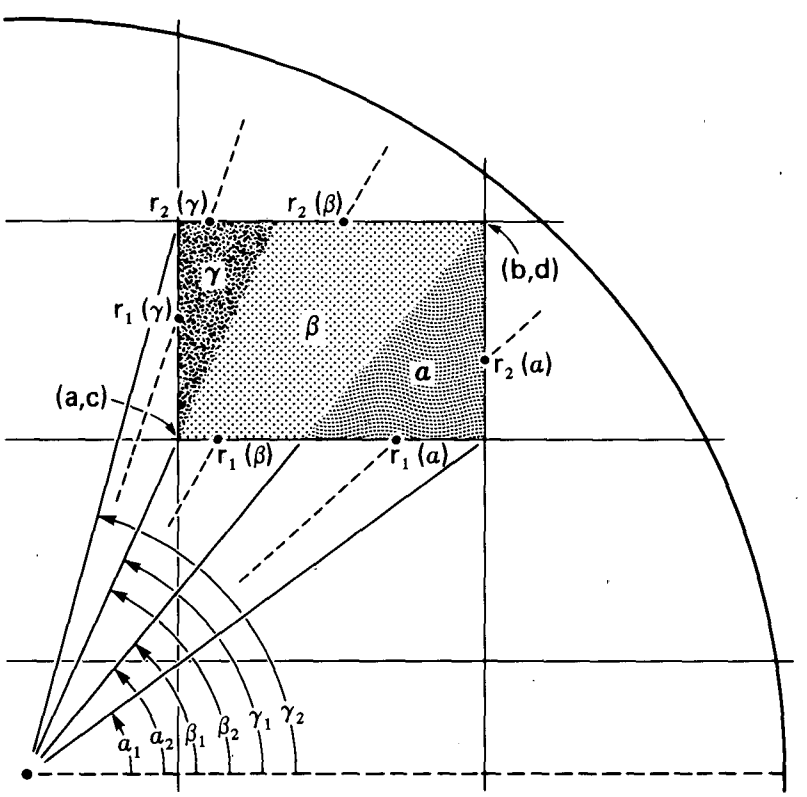


FIG. 2. Model for calculating the view-factor of a rectangular pixel within a circular image.

A number of alternative positions of pixels in the image occurs, necessitating a different formulation of Eq. (6) for each position. The computational details of this aspect of the technique are given in Johnson and Watson (1985b), along with listings of FORTRAN 77 routines necessary to compute $\psi_P$.

Calculation of $\psi_P$ in this manner produces an error by virtue of the fact that only those pixels which lie *within* the circular fish-eye lens image are considered. Because the pixels are rectangular, it is inevitable that some will not lie wholly within the circular image, causing errors in $\psi_P$ for pixels near the edge of the image. Although the cosine term in (1) means that $\psi_P$ are small near the image boundaries, the accumulated error may be significant if the pixel array is small. One way to estimate the extent of this error is to sum $\psi_P$ for all pixels which lie *entirely* within the image: in the case of no error the total should equal unity. Figure 3 shows that the error decreases as the size of the pixel array increases and eventually becomes insignificant ($3.6 \times 10^{-4}$%) for the 256 × 256 array used in this study.

The technique described above yields a view-factor array that matches the pixel array produced by the frame-store device. That is, an element of the view-factor array corresponds exactly with the equivalent pixel in the image array in terms of its aspect ratio, and location with respect to the center of the fish-eye lens image.

## 3. Image generation and analysis

### *a. Image generation*

The pixel arrays representing images of urban skylines were generated using readily available video technology and a custom-made lens-to-camera adaptor. The fish-eye lens used was a standard Canon 28 mm, f/5.6 model attached to a Panasonic WV-1950 television camera. The field of view of this lens is 180°. The custom-made adaptor contained a focal-plane diaphragm and two filter holders for image brightness control. The images were stored on a video cassette recorder (Sony, model SL0323) for subsequent analysis. Prior to recording the images, the camera was mounted on a tripod and leveled. During field operation the equipment was powered by a small portable generator (Honda, Model 800V), an arrangement that proved simple and efficient to operate in a variety of conditions.

The recorded images were subsequently replayed into a video frame store (Colorado Video, model 274D), which was utilized in "frame-grab" mode to digitize an image into an array of 256 × 256 pixels with a greyscale of 256 brightness levels.

### *b. Image analysis*

It is necessary to subject each 256 × 256 pixel image to an analytic procedure that can distinguish between

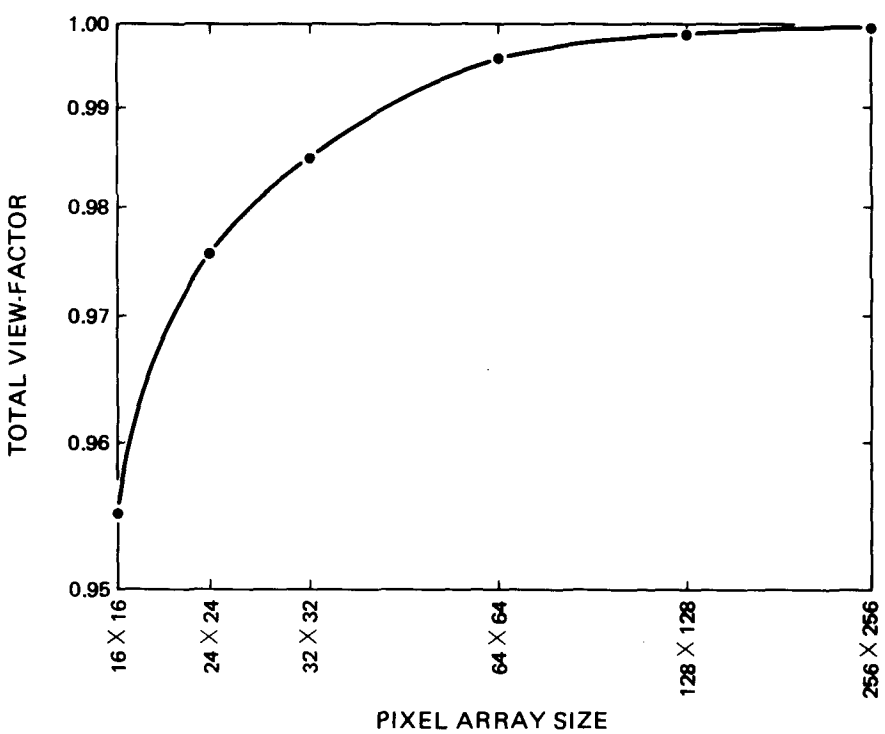


FIG. 3. Total view-factor for all pixels lying entirely within a circular image, according to the size of the pixel array.

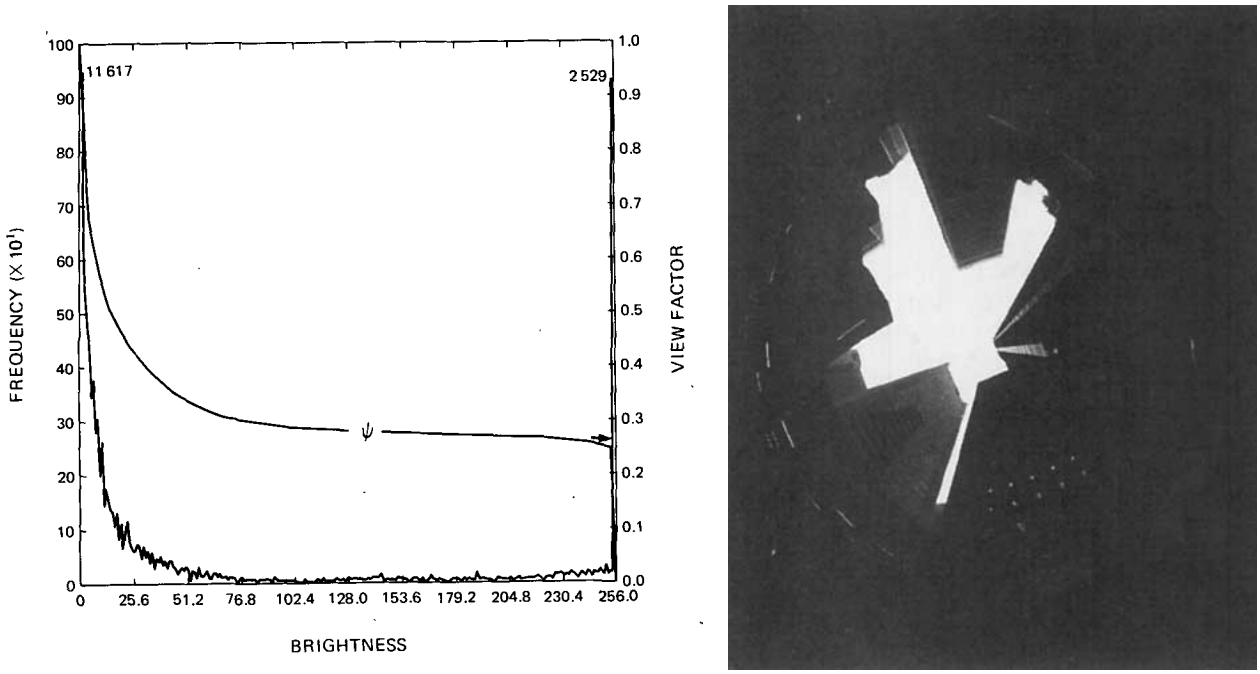


FIG. 4. Case 1. Fish-eye lens image and frequency distribution of pixel brightnesses. The curve labeled $\psi$ shows the cumulative view-factor as a function of the global brightness threshold used. The jagged curve shows the frequency distribution of brightnesses in the image used to generate the $\psi$ curve. The two numbers are the frequencies of pixels having brightnesses of 0 and 255 respectively. The arrow indicates $\psi_S$ as determined by the Johnson and Watson (1984) technique.

pixels representing sky and those representing nonsky. This problem is a simple case of a general class of problems conventionally called "image segmentation" (Pavlidis, 1982), whereby pixels representing common features of an image are identified: here, the "segments" are either sky or nonsky.

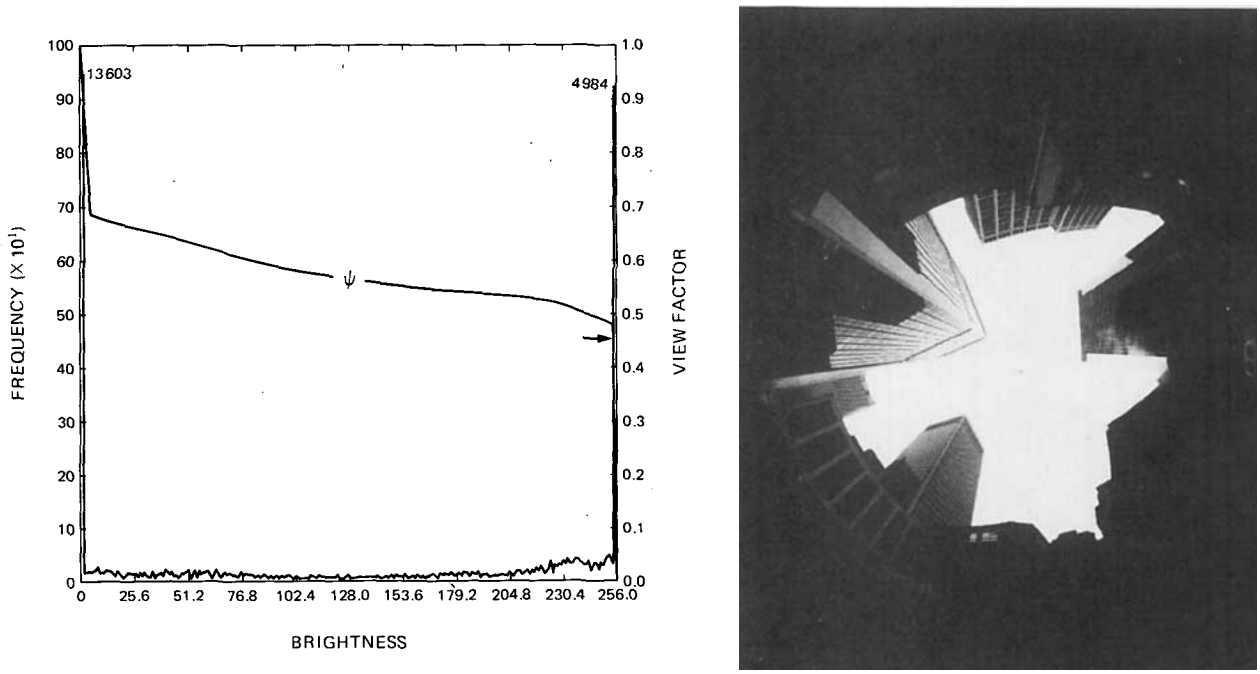


FIG. 5. As in Fig. 4 but for Case 2.

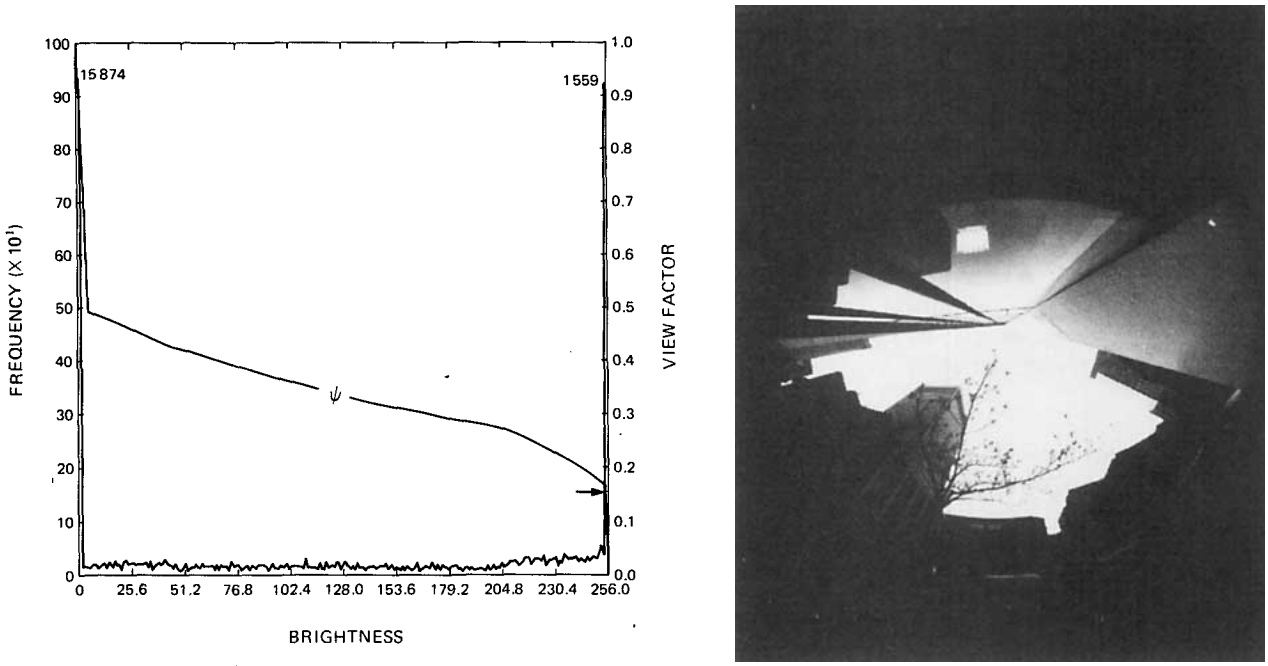


FIG. 6. As in Fig. 4 but for Case 3.

In the present application, we will use the simplest method for image segmentation. This method uses a global threshold as the sole means to distinguish between sky and nonsky. We consider this to be a reasonable approach if steps are taken to ensure that, as far as possible, brightness is the distinguishing feature of sky and nonsky. This can be arranged by acquiring data under completely overcast conditions so as to reduce the possibility of specular reflections from nonsky objects. The further measure of adjusting the lens aperture and/or filter density to saturate (the electronic equivalent of photographic overexposure) sky pixels will add to the robustness of the global threshold technique. The latter effect may also be achieved by adjusting the gain on the frame-store device.

The correct determination of a global threshold is crucial to the success of the present technique. If the image brightnesses are manipulated as suggested, the frequency distribution of brightnesses will be bimodal. In the extreme (most desirable) case, this bimodality will consist of a large peak at or above the minimum brightness and one at or below the maximum brightness. In the present application, the latter represents sky pixels and the former represents nonsky pixels. The intermediate brightness values represent pixels that are not unambiguously sky or nonsky. While aperture manipulation will serve to reduce the number of pixels with intermediate brightness, the proper assignment of these pixels can only be made by more sophisticated image analysis techniques (e.g., Brice and Fennema, 1970).

While the intent of the present contribution is to develop a technique based on video technology, it must be pointed out that analysis of the image is independent of its generation. It is possible to apply the same analysis to images generated by a scanning optical densitometer from negatives of fish-eye lens photographs, an approach employed by McArthur and Hay (1981) in a different context.

### c. *Summary*

Specification of "sky" pixels in a video image by applying an appropriate global brightness threshold produces a subset of pixels

$$S = \{P_{ij} : P_{ij} \text{ has brightness greater than threshold}\}$$

where $P_{ij}$ is the pixel in row $i$ and column $j$ of the video array. We may now give the sky view-factor as

$$\psi_S = \sum_{P_{ij} \in S} \psi_{P_{ij}},$$

where $\psi_{P_{ij}}$ is the view-factor of each pixel in the view-factor array as described in section 2.

## 4. Discussion

The application of the technique described above will be illustrated with reference to three cases. In each case the sky view-factor, $\psi_S$, determined from the video technique, will be compared with $\psi_S$ calculated independently using the approach of Johnson and Watson (1984), whereby a view-factor is calculated for each wall in a photographic image.

### a. *Case 1*

The most straightforward case is illustrated in Fig. 4 where the image shows a marked difference between

sky and buildings. A brightness frequency distribution (Fig. 4) shows that most of the video image is comprised of the lowest 20% of brightness levels, representing the building surfaces. The frequency of darker pixels is offset by a pronounced peak at the top brightness level which represents the sky. In cases such as this where the frequency distribution is so distinctly bimodal, there is little difficulty in distinguishing between sky and buildings on the basis of a global brightness threshold. If the threshold is such that $\psi_P$ are determined only for pixels with the highest brightness level (255), the $\psi_S = 0.25$, a result that differs by a mere 2% from the independently determined $\psi_S$.

*b. Case 2*

In the second example (Fig. 5), the distinction between sky and buildings is less clear than in Case 1 because the nature of the building surfaces and more open skyline has increased the degree of specular reflection. The distribution of brightness levels in Fig. 5 bears this out with an increased frequency of pixels at the higher end of the range. However, their greater frequency is insufficient to detract from the dominance of the highest brightness level and, when $\psi_P$ are summed for these pixels, they give a sky view-factor of 0.48. This result compares favourably with 0.46 given by the Johnson and Watson (1984) technique.

*c. Case 3*

The third example has been included to illustrate some of the problems which may beset the technique. Figure 6 shows that the distinction between sky and building is rendered more ambiguous because of considerable reflection from glass surfaces, intrusion of bright lights from within buildings, and by the presence of foliage. The distribution of brightness levels (Fig. 6) shows that the additional diffuse radiation has increased the frequency of brightness levels across the entire range, but particularly at higher brightnesses. Despite the complexity of the case 3 image, the highest brightness level still dominates and gives a sky view-factor of 0.16, which is within 1% of the result calculated independently.

Results for the three cases presented here suggest that a global brightness threshold is a sufficiently robust means of distinguishing between sky and buildings, providing that the video image is manipulated carefully. The most important procedure in this regard is to "saturate" sky pixels either by aperture control or at the frame-store device so that the highest brightness level represents "sky." At this stage the operator applies to the raw data an unspecified transform that is crucial to the success of the method.

## 5. Conclusions

The technique presented appears capable of providing a quick and convenient determination of sky view-factors in urban environments, regardless of the complexity of the skyline. In order to apply the technique, a video image acquired through a fish-eye lens is required. This image (as a digitized array of pixels) is analysed to discriminate between sky and nonsky pixels, and the sky view-factor is determined by summing the numerically determined view-factors for all sky pixels. The technique is potentially useful when view-factors are required for a large number of locations. The limitations of the present technique are related to the way in which the sky/nonsky pixel discrimination is achieved. The present global threshold technique depends on an electronic manipulation of the video image (a gain and/or dynamic range adjustment is all that is required). This limitation may be removed at the expense of added image analysis software.

Listings of numerical algorithms, and the report by Johnson and Watson (1985b) are available from the senior author upon request.

*Acknowledgments.* This work was partially funded by grants from the Natural Science and Engineering Research Council of Canada. Muriel March and Sandy Pan typed the manuscript while Paul Jance drafted the diagrams.

REFERENCES

Anderson, M. C., 1964: Studies of Woodland light climate. *J. Ecol.*, **52**, 27–41.

Brice, C. R., and C. L. Fennema, 1970: Scene analysis using regions. *Artif. Intell.*, **1**, 205–226.

Johnson, G. T., and I. D. Watson, 1984: The determination of view-factors in urban canyons. *J. Climate Appl. Meteor.*, **23**, 329–335.

——, and ——, 1985a: Reply to "Comments on the determination of view-factors in urban canyons." *J. Climate Appl. Meteor.*, **24**, 386 pp.

——, and ——, 1985b: Calculating view-factors using video imagery. Tech. Rep. No. 85-015, School of Mathematics and Physics, Macquarie University, 25 pp.

McArthur, L. B., and J. E. Hay, 1981: A technique for mapping the distribution of diffuse solar radiation over the sky hemisphere. *J. Appl. Meteor.*, **20**, 421–429.

Oke, T. R., 1981: Canyon geometry and the nocturnal urban heat island: Comparison of scale model and field observations. *J. Climatol.*, **1**, 237–254.

Pavlidis, T., 1982: *Algorithms for Graphics and Image Processing.* Springer-Verlag, 416 pp.

Steyn, D. G., 1980: The calculation of view factors from fish eye lens photographs. *Atmos.-Ocean*, **18**, 254–258.

——, and T. J. Lyons, 1985: Comments on "The determination of view-factors in urban canyons." *J. Climate Appl. Meteor.*, **24**, 383–385.